International Journal of Rock Mechanics & Mining Sciences 138 (2021) 104622

Contents lists available at ScienceDirect

International Journal of Rock Mechanics and Mining Sciences

journal homepage: http://www.elsevier.com/locate/ijrmms

Stress wave superposition effect and crack initiation mechanism between two adjacent boreholes

Chenxi Ding [a,b], Renshu Yang [a,c,*], Chun Feng [d]

[a] School of Civil and Resource Engineering, University of Science and Technology Beijing, Beijing, 100083, China
[b] Failure Mechanics & Engineering Disaster Prevention and Mitigation, Key Laboratory of Sichuan Province, Sichuan University, Chengdu, 610065, China
[c] State Key Laboratory for Geomechanics and Deep Underground Engineering, Beijing, 100083, China
[d] Key Laboratory for Mechanics in Fluid Solid Coupling Systems, Institute of Mechanics, Chinese Academy of Sciences, Beijing, 100190, China

ARTICLE INFO

Keywords:
Blasting
Stress wave superposition
Crack initiation
Digital image correlation
Model experiment
Numerical simulation

ABSTRACT

In rock blasting, the effect that stress wave superposition between boreholes has on rock fragmentation remains controversial. Here, we experimentally study the stress wave superposition effect between two adjacent boreholes by combining the model experiment method and the high-speed digital image correlation experimental system. Numerical simulations based on the continuous-discontinuous element method are also used to analyze the crack initiation mechanism between two adjacent boreholes. The model experiment results show that, in the stress wave superposition area between boreholes, the stress component in the direction of the connection line of the two boreholes is mainly compressive, while that in the direction perpendicular to the connection line is mainly tensile. Superposition of the blasting stress waves between the boreholes strengthens both stress components, but the strengthening effect on the stress component in the direction perpendicular to the connection line (mainly tensile) is significantly less than that in the direction of the connection line (mainly compressive). Moreover, these stress enhancements are not sufficient to induce crack initiation in the stress wave superposition area between boreholes. Numerical simulation analysis further shows that crack initiation in the stress wave superposition area has relatively stringent requirements on the explosive parameters, rock properties and borehole spacing, which are difficult to observe in engineering practice and model experiments.

1. Introduction

The drilling and blasting method exploits an instantaneous release of explosive energy to achieve efficient fragmentation of rock, and is widely used in many fields such as mining engineering,[1–3] traffic engineering,[4,5] hydropower and nuclear power infrastructure.[6,7] The borehole pressure, stemming material, boundary condition, delay time and the complicated stress-wave interaction during the blast play a significant role.[8–10] In engineering practice, the process of rock blasting requires that multiple boreholes be detonated simultaneously or in a delayed fashion. The interaction of blasting stress waves among multiple boreholes is an important factor affecting the blasting effect. Rossmanith et al.[11,12] performed a simplified two-dimensional model that suggested that the superposition of blasting stress waves had a positive effect on rock fragmentation in smooth blasting and bench blasting. Based on the interaction of the blasting stress waves, Vanbrabant et al.[13] noted that a reasonable blasting delay time should be chosen to reinforce wave tensile tails between the boreholes, thereby increasing the fracture degree of the rock. The influence of the location of the guide hole between the two boreholes and the initiation time lag on the crack propagation control was discussed by Cho et al.[14] Additionally, research by McKinstry et al.,[15] Lewis et al.[16] and Khandelwal et al.[17] shows that the delay time can control the mutual superposition effect of blasting stress waves between the boreholes, which can effectively reduce the blasting vibration speed and improve rock fragmentation. Therefore, many researchers and previous works suggest that the superposition of stress waves between boreholes improves rock fragmentation efficiency in rock blasting.

However, with the deepening of research in recent years, many researchers have raised objections to this suggestion. Among these, the investigation by Katsabanis et al.[18] indicated that selecting a very short delay time for optimization of fragmentation is questionable. High speed

Abbreviations: CDEM, continuous-discontinuous element method; DIC, digital image correlation; PC, polycarbonate.

* Corresponding author. School of Civil and Resource Engineering, University of Science and Technology Beijing, Beijing, 100083, China.
E-mail address: yrs@cumtb.edu.cn (R. Yang).

https://doi.org/10.1016/j.ijrmms.2021.104622
Received 12 March 2020; Received in revised form 2 November 2020; Accepted 31 December 2020
Available online 9 January 2021
1365-1609/

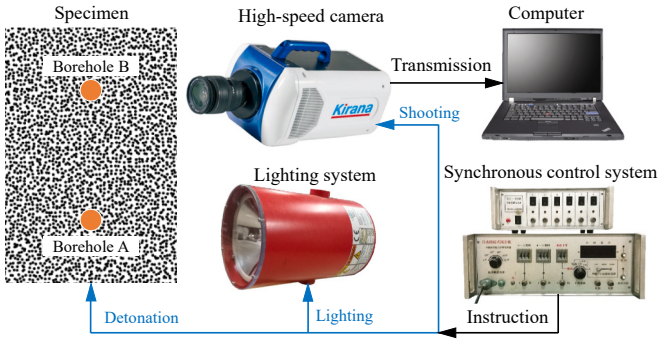

Fig. 1. High-speed DIC experimental system.

analysis of the small-scale tests suggested that the optimum fragmentation occurs well past the time, where the action of stress waves is possible.[19] After a detailed review of past data and a theoretical analysis with an advanced analytic model, Blair[20] stated that the role of stress wave superposition in rock fragmentation by blasting was neither predictable nor significant. He also believed that the assumptions used in previous research studies supporting stress wave superposition to improve rock fragmentation efficiency were very limited. Similarly, the results of model experiments[21] and numerical simulations[22,23] show that stress wave superposition between boreholes controlled by delay blasting has no significant effect on rock fragmentation. Additionally, Yue et al.[24] and Wang et al.[25] used the caustics method to study the crack propagation behavior of the defective medium under the action of a blasting stress wave; many of their experimental results show that the cracking does not preferentially initiate in the stress wave superposition area between the boreholes. These reports also raise significant doubts regarding the traditional view that the blasting stress wave superposition makes the crack preferentially propagate.

Much controversy thus remains regarding the effect of the blasting stress wave superposition on rock fragmentation. Therefore, it is necessary to conduct a more in-depth study on the superposition effect of blasting stress waves and the mechanism of crack initiation caused by the stress wave superposition. To this end, this paper combines a model experiment and the digital image correlation (DIC) method to quantitatively study the stress wave superposition effect between two adjacent boreholes. Additionally, the crack initiation mechanism in the stress wave superposition area between two adjacent boreholes is further discussed according to the analysis results of the model experiments based on a numerical simulation using the continuous-discontinuous element method (CDEM).

2. Model experiment design based on DIC method

The DIC method[26–28] calculates the correlation coefficient of the gray value of a speckle image on the surface of a specimen before and after a deformation. This method tracks the spatial position of the calculated point before and after deformation, and obtains the surface displacement of the specimen and, ultimately, the strain information. Based on the basic principles of the DIC method, the high-speed DIC experimental system was established herein (Fig. 1), and was primarily composed of a high-speed camera, a lighting system, and a synchronous control system. This high-speed DIC system can realize quantitative results of the strain evolution of super-dynamic problems such as blasting.[29] In particular, the self-designed synchronous control system can control the starting sequence of the high-speed camera, the lighting system and the detonation device; and realize microsecond-scale control of the detonation time suitable for simultaneous and delayed detonations of multiple boreholes.

This model experiment mainly studies the strain characteristics and stress evolution trend of stress wave superposition between two adjacent boreholes. Therefore, it is necessary to avoid the occurrence of blast-induced cracks. For this reason, polycarbonate (PC), which possesses a superior toughness, was used as the material of the model experiment; and lead azide ($Pb(N_3)_2$), which possesses a small blasting pressure, was used as the explosive with explosive charges of only 100 mg per borehole. The explosive in the borehole was detonated by a high-voltage discharge via metal probes. The dimensions of the model specimen shown in Fig. 1 are 500 mm × 300 mm × 5 mm. Boreholes A and B had 4-mm diameters and were prefabricated in the middle of the specimen with a distance between the two boreholes of 200 mm. The speckle pattern deposited on the model specimen surface had a speckle diameter of 1.2 mm, a speckle density of 75%, and a speckle irregularity of 75%. Relevant material parameters of the PC are listed in Table 1. Each experiment was repeated three times. By strictly controlling the charge density and borehole blockage, the experimental results are guaranteed to have good repeatability.

Table 1
Material parameters of the polycarbonate (PC) used in this study.

Dynamic elastic modulus /GPa	Dynamic shear modulus /GPa	Dynamic Poisson ratio	P-wave velocity /m·s^{-1}	S-wave velocity /m·s^{-1}	Density /kg·m^{-3}
4.548	1.722	0.321	2125	1090	1449

3. Model experiment of stress wave superposition effect between two adjacent boreholes

3.1. Simultaneous detonation

For the condition wherein the boreholes A and B were simultaneously detonated, the detonation time was recorded as $t = 0$. Fig. 2 shows the von Mises strain cloud measured at various times after $t = 0$. For a planar problem, the von Mises strain comprehensively considers the maximum and minimum principal strains and can more comprehensively reflect the strain state of the specimen. It can be seen from Fig. 2 that, after simultaneous detonation of the two boreholes, the blasting stress waves spread around the boreholes. At $t = 57$ μs, the blasting stress wave columns from each of the boreholes begin to meet and then superpose. At $t = 68$ μs, the superposition of the two wave columns continues to strengthen, and the strain at the position where the stress waves are superposed increases remarkably. After $t = 68$ μs, the two waves pass each other and continue to spread. As the blasting energy dissipates, the specimen strain continues to decay.

Some gauging points were selected, as shown in Fig. 3, where gauging point M was located at the midpoint of the connection line of the two boreholes (i.e., $x = 0$), where the direction along the connection line of the two boreholes was defined as the x-direction. The six gauging points on the left side of M were respectively labeled as L1, L2, ..., L6, and the six gauging points on the right side of M were respectively labeled as R1, R2, ..., R6. The distance between adjacent gauging points was 10 mm, the distance between L6 (located at $x = -60$ mm) and borehole A (located at $x = -100$ mm) was 40 mm, and the distance between R6 and borehole B was 40 mm. The direction perpendicular to the connection line was defined as the y-direction.

Because the selected gauging points were relatively far from the borehole, the strain at each gauging point was recovered without residual strain after the action of the blasting stress wave. That is to say, the stress states of the selected gauging points were within the elastic limit, and the relationship between the stress and strain components of the gauging points satisfied the equation

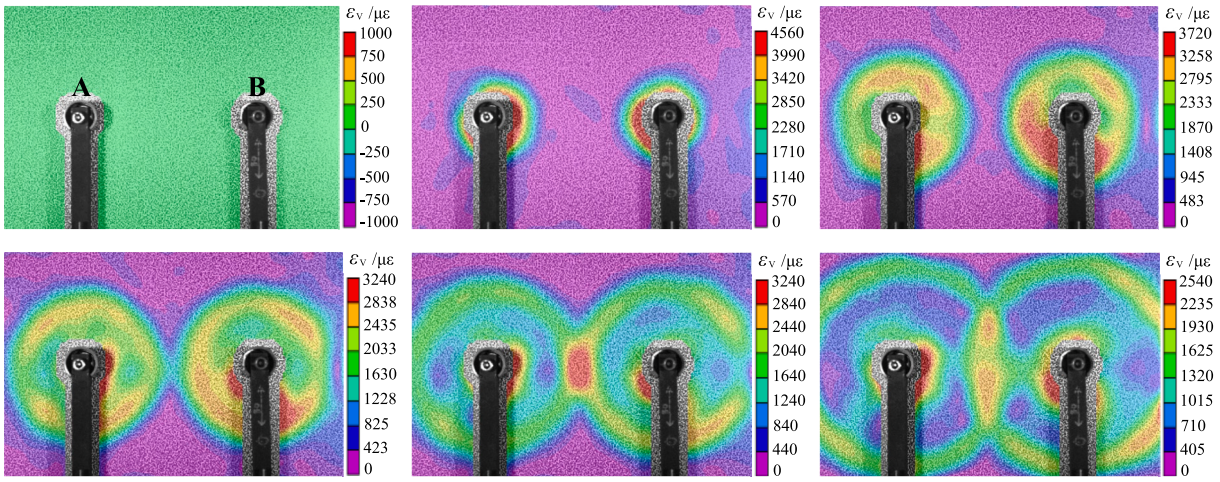

Fig. 2. von Mises strain clouds for simultaneous detonation of two boreholes at $t = 0$ μs, showing the strain clouds (left to right) at $t = 0$, 30, 50 (upper images), 57, 68, and 83 μs (lower images).

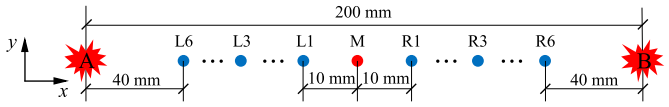

Fig. 3. Diagram of the gauging point and borehole positions.

$$\begin{cases} \sigma_x = \dfrac{E_d}{1-\upsilon^2}\left(\varepsilon_x + \upsilon\varepsilon_y\right) \\ \sigma_y = \dfrac{E_d}{1-\upsilon^2}\left(\varepsilon_y + \upsilon\varepsilon_x\right) \end{cases}, \tag{1}$$

where σ_x and σ_y are the stress components in the x and y directions, respectively; ε_x and ε_y are the strain components in the x and y directions, respectively; E_d is the dynamic elastic modulus; and υ is the dynamic Poisson ratio.

When the boreholes A and B were simultaneously detonated, the stress states of the gauging points on the left and right sides of gauging point M were symmetric. Therefore, for simplicity and brevity, only gauging point M and the two left gauging points L3 and L6 were selected for analysis. Using the strain components of the relevant gauging points and Eq. (1), the stress components as a function of time at gauging points M, L3 and L6 were obtained and are shown in Fig. 4. The stress value is positive for a tensile stress and negative for a compressive stress. It can be seen from Fig. 4 that the stress component σ_x is mainly compressive and the stress component σ_y is mainly tensile.

Stress component σ_x: Gauging point L6 is first subjected to the blasting stress wave from borehole A, where σ_x reaches its peak value of −17.6 MPa at $t = 33$ μs and then gradually decays. Next, L6 is affected by the blasting stress wave from borehole B, where σ_x reaches its secondary peak value of −10.9 MPa at $t = 108$ μs. Similarly, gauging point L3 is first subjected to the blasting stress wave from borehole A, where σ_x reaches its peak value of −10 MPa at $t = 51$ μs. Next, L3 is affected by the blasting stress wave from borehole B, where σ_x reaches its secondary peak value of −6.5 MPa at $t = 92$ μs. Gauging point M is simultaneously subjected to the blasting stress waves of both boreholes, which simultaneously propagate to M and superpose to reach a peak σ_x value of −18.3 MPa at $t = 68$μs.

Stress component σ_y: Gauging point L6 is first subjected to the blasting stress wave from borehole A, where σ_y reaches its peak value of 8.5 MPa at $t = 52$ μs and then gradually decays. Next, L6 is affected by the blasting stress wave from borehole B, where σ_y reaches its secondary peak value of 3.5 MPa at $t = 132$ μs. Similarly, gauging point L3 is first subjected to the blasting stress wave from borehole A, where σ_y reaches its peak value of 3.7 MPa at $t = 70$ μs. Next, L3 is affected by the blasting stress wave from borehole B, where σ_y reaches its secondary peak value of 2.8 MPa at $t = 110$ μs. Gauging point M is simultaneously subjected to the blasting stress waves of both boreholes, which simultaneously propagate to M and then superpose to reach a peak σ_y value of 5.1 MPa at $t = 96$ μs.

The above stress analysis of the gauging points shows that, under the action of the blasting stress wave, at the same gauging point, the maximum absolute value of the compression phase (i.e., the peak value σ_{px}) of the stress component σ_x is significantly larger than the maximum absolute value of the tension phase (i.e., peak value σ_{py}) of the stress component σ_y. Therefore, the stress state of the gauging point is

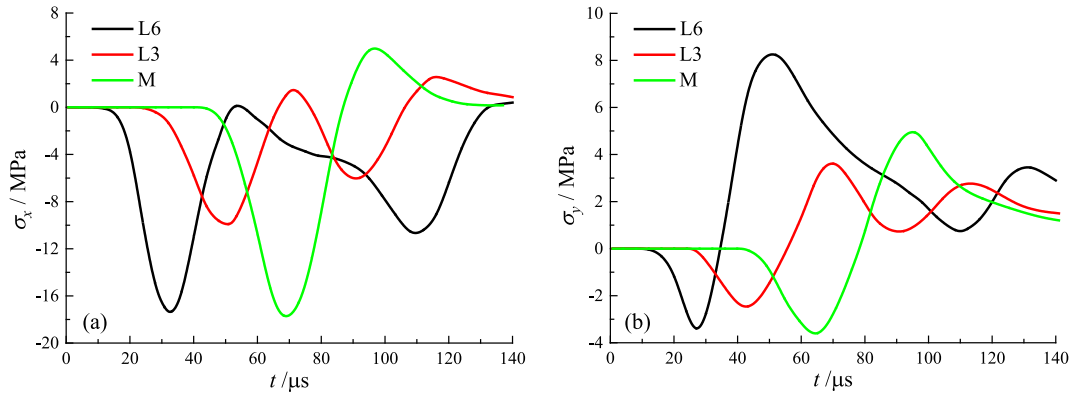

Fig. 4. Stress component σ vs. time after simultaneous detonation of two boreholes, showing (a) x-component of stress σ_x, and (b) y-component of stress σ_y.

Table 2
Stress component peaks of the gauging points in the condition that the two boreholes are simultaneously detonated.

The gauging point	L6	L5	L4	L3	L2	L1	M	R1	R2	R3	R4	R5	R6
σ_{px} /MPa	−17.6	−14.7	−12.1	−10.0	−10.4	−14.2	−18.3	−14.0	−10.4	−10.2	−12.6	−15.5	−18.2
σ_{py} /MPa	8.5	6.3	4.7	3.7	3.6	4.3	5.1	4.3	3.6	3.7	4.7	6.2	8.4

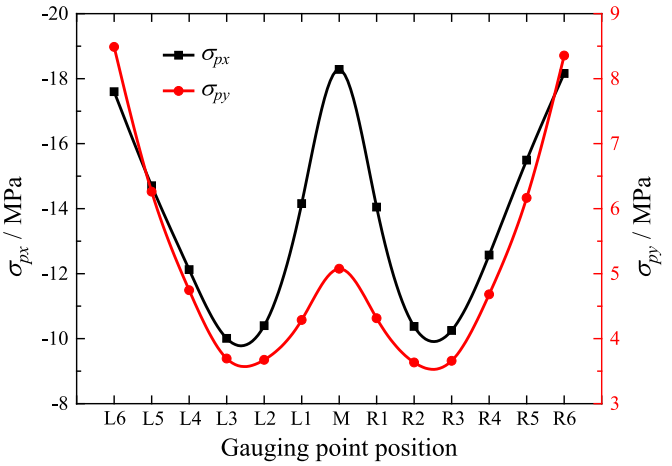

Fig. 5. Stress component peak value of the compression phase (σ_{px}) (left axis) and the tension phase (σ_{py}) (right axis) vs. position of the gauging point for simultaneous detonation of two boreholes.

primarily compressive in the x-direction and auxiliary tensile in the y-direction.

Using the plots of the stress components σ_x and σ_y as a function of time after detonation for all of the gauging points (similar to that in Fig. 4 shown for gauging points L6, L3 and M only), the stress component peaks σ_{px} and σ_{py} of all of the gauging points were obtained, and are given in Table 2 and Fig. 5. It can be seen from Fig. 5 that the superposition of blasting stress waves between the boreholes has a significant influence on the stress state at the gauging points, and the stress component peak of the gauging points along the connection line of the two boreholes (i.e., $y = 0$) exhibits a "W"-type distribution. Along the connection line of the two boreholes (i.e., $y = 0$), the area between gauging points L3 and R3 is where the stress is apparently superposed. In this area, the stress superposition is greater than the natural attenuation of the blasting stress. Gauging point M (i.e., $x = 0$, $y = 0$) is the position where the two blasting stress wave columns meet and the stress superposition is strongest, while gauging points L3 (i.e., $x = -30$ mm, $y = 0$) and R3 (i.e., $x = 30$ mm, $y = 0$) are the two inflection points of the change in the stress component peak. Compared with the stress component peaks at gauging points L3 and R3, the stress component peak of gauging point M is increased by 79–83% for σ_{px} and by about 38% for σ_{py}. Therefore, the superposition of blasting stress waves strengthens the compression phase in the x-direction significantly more than the tension phase in the y-direction.

In rock blasting, rock located in areas far from the borehole mainly undergoes tensile failure under the action of the blasting stress wave. The above analysis results show that the reinforcement of the tensile stress between the boreholes is not significant enough to cause tensile damage to the specimen. Although the superposition of blasting stress waves between the boreholes significantly enhances the compressive stress, it is still much smaller than the compressive strength of the specimen, and it is difficult to change the failure mode of the specimen from tensile failure to compression failure.

3.2. Delayed detonation

For the condition wherein the boreholes A and B experience delayed detonation, there was a very short delay between the detonation of borehole A ($t = 0$) and the subsequent detonation of borehole B, where the delay time Δt of the borehole B detonation varied as 10, 20, 30 and 40 μs. For simplicity and brevity, Fig. 6 only shows the von Mises strain clouds after borehole B detonation delay times Δt of 20 and 40 μs. For the delay time $\Delta t = 20$ μs, the two blasting stress wave columns begin to meet and superpose between the two boreholes at $t = 67$ μs and reach their maximum at $t = 77$ μs. Similarly, in the condition that the delay time Δt of the borehole B is 40 μs, the two columns of blasting stress waves begin to meet and superpose between the two boreholes at $t =$ 67μs and reach their maximum at $t = 95$μs. Subsequently, the blasting stress waves gradually decay and continue to spread.

Fig. 7 shows a comparison of the stress component peak of each gauging point during the conditions of simultaneous ($\Delta t = 0$ μs) and delayed ($\Delta t > 0$ μs) detonation. It can be seen in Fig. 7 that for delayed detonation the superposition of the blasting stress waves between the boreholes shows a similar trend to that for simultaneous blasting. Namely, the stress wave superposition strengthens the stress component peak σ_{px} significantly more than σ_{py}.

As the detonation delay time Δt at borehole B increases, the area where the two blasting stress wave columns meet gradually moves to the right. Correspondingly, the position of the gauging point corresponding to the stress superposition peak between the two boreholes also gradually moves to the right. Table 3 lists the superposed stress component peaks and their corresponding gauging points between the two boreholes for the various blasting conditions. With increasing detonation delay time Δt at borehole B, the stress component peak of the stress superposed area initially decreases and then increases, and the stress wave from borehole B gradually strengthens the stress superposition between the boreholes.

Traditional rock blasting theory posits that cracks are preferentially generated at positions where the stresses are superposed between the boreholes, but this phenomenon is rarely observed in actual blasting engineering and model experiments. The different effects that stress wave superposition has on the compression and tension phases of the stress component are analyzed above, and the reason for the difficulty of understanding this phenomenon is explained from the perspective of the stress action characteristics. It will be further studied in the following by numerical simulation, whereby the necessary conditions for crack initiation and propagation in the stress wave superposition area between boreholes are discussed.

4. Numerical simulation on stress wave superposition cracking between two adjacent boreholes

4.1. CDEM and the establishment of blasting numerical model

The continuous-discontinuous element method (CDEM) is an explicit dynamic numerical analysis method in which a finite element and a discrete element are coupled.[30,31] The method is typically used to simulate the progressive failure process of rock and can reproduce the entire process of crack initiation, propagation and penetration. As shown in Fig. 8, the numerical model in CDEM comprises the two parts of a block and an interface. A block consists of one or more finite elements that represent the continuous characteristics of the material such as elasticity and plasticity. The common boundary between two blocks is the interface, which is used to represent the discontinuous characteristics such as fracture, slip, and collision of the material. Additionally, the interface includes a real interface and a virtual interface. The real

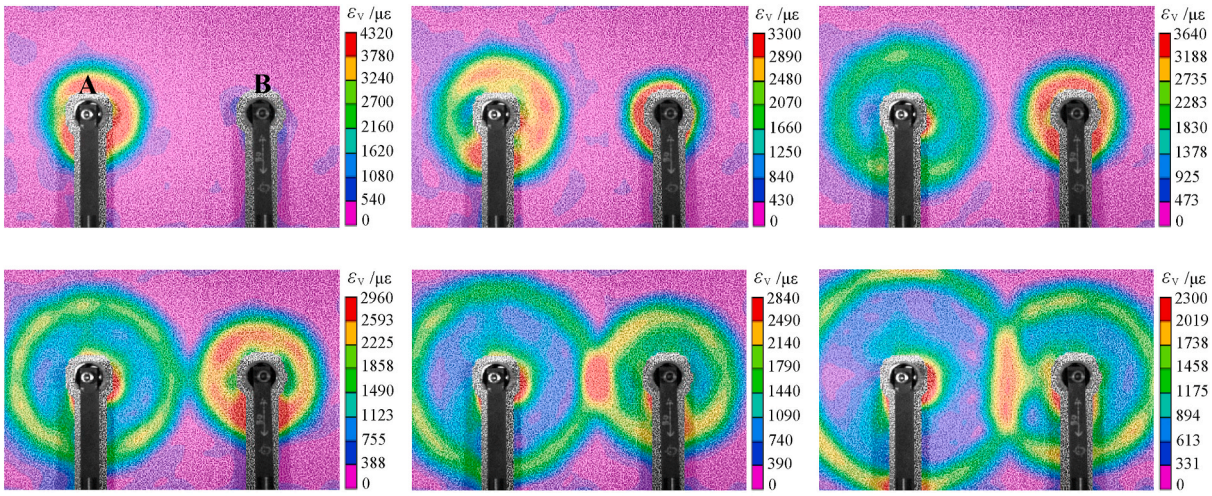

(a) Detonation delay time Δt of 20 μs

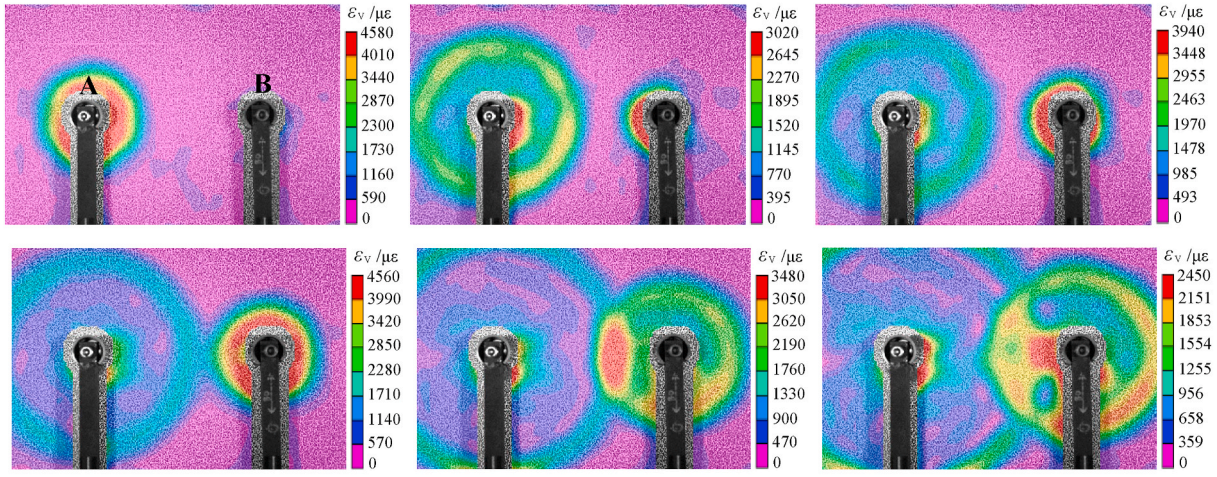

(b) Detonation delay time Δt of 40 μs

Fig. 6. von Mises strain clouds for delayed detonation of two boreholes, for a detonation delay time Δt of (a) 20 μs and (b) 40 μs. The images in (a) show the strain clouds (left to right) at $t = 40$, 50, 60 (upper images), 67, 77, and 92 μs (lower images). The images in (b) show the strain clouds (left to right) at $t = 40$, 65, 70 (upper images), 77, 95, and 105 μs (lower images).

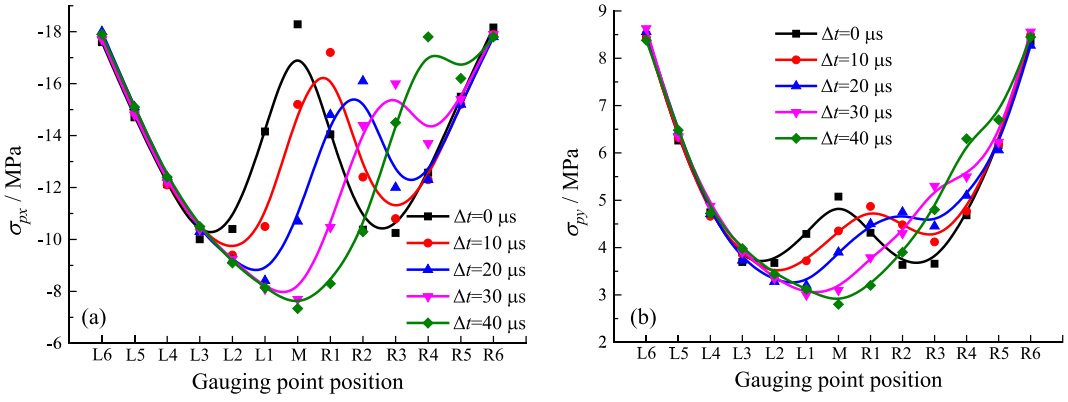

Fig. 7. Stress component peak value of the (a) compression phase (σ_{px}) and (b) tension phase (σ_{py}) vs. position of the gauging point for various blasting conditions.

interface is used to represent real discontinuities such as internal joints, cracks and faults. The virtual interface mainly provides a potential path for the propagation of explicit cracks. The virtual interface connects the solid elements on both sides through the normal penalty spring and the tangential penalty spring and transmits the mechanical information. The tensile fracture process and the shear fracture process can be realized on

Table 3
Stress component peaks of the compression phase (σ_{px}) and the tension phase (σ_{py}) and their corresponding gauging points.

Delay time Δt	0μs (Simultaneous)	10μs	20μs	30μs	40μs
σ_{px} /MPa	−18.3	−17.2	−16.1	−16	−17.8
σ_{py} /MPa	5.1	4.9	4.8	5.3	6.3
Corresponding gauging point	M	R1	R2	R3	R4

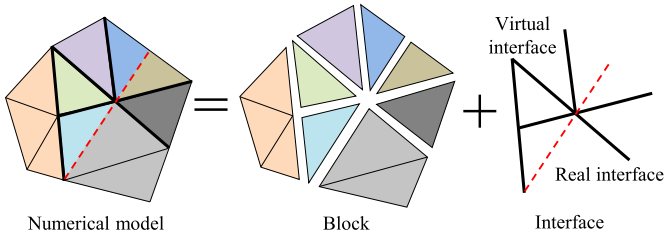

Fig. 8. Numerical model composition in CDEM.[32]

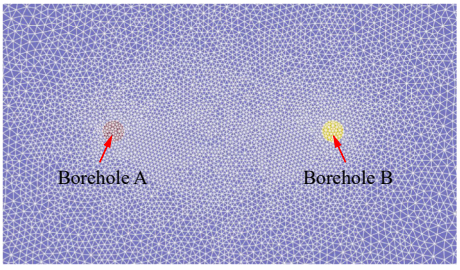

Fig. 9. Mesh around the boreholes for the numerical model with borehole spacing $\Delta l = 60$ mm.

the virtual interface by setting the fracture criterion and the corresponding strength parameter on the penalty spring. After the fracture occurs, the virtual interface is transformed into a real interface.

A two-dimensional blasting numerical model with two boreholes was established with a model size of 500 mm × 300 mm and a borehole diameter of 4 mm. To study the influence of borehole spacing Δl on crack initiation in the stress wave superposition area between two boreholes detonated under the same conditions, two numerical models were established with the borehole spacing varying as $\Delta l = 60$ and 90 mm. Fig. 9 shows the mesh around the borehole in the numerical model with $\Delta l = 60$ mm, where the total number of nodes in the numerical model was 18278 and the total number of elements was 36234. The boundary of the model was set as a non-reflective boundary.

Modeling the explosive uses the Landau model, such that

$$\begin{cases} pV^{\gamma} = p_0 V_0^{\gamma}, & p \geq p_k \\ pV^{\gamma_1} = p_k V_k^{\gamma_1}, & p < p_k \end{cases}, \tag{2}$$

where p and V are the transient pressure and volume of the high pressure gas, respectively; p_0 is the detonation pressure; V_0 is the charge volume; p_k and V_k are the pressure and volume of the high-pressure gas at the boundary of the two adiabatic processes, respectively; and γ and γ_1 are the adiabatic indices of the blasting gas in the initial and second stages, respectively.

Under a blasting load, the rock mass breaks and forms through-cracks. The blasting gas in the borehole overflows quickly from the through-crack, which causes the pressure in the borehole to drop sharply. Because the direct simulation of the flow and overflow process of the blasting gas in the rock mass is complicated, an equivalent

Table 4
Relevant parameters of the explosive used in the numerical simulation.

Detonation heat /J·kg^{-1}	Detonation velocity /m·s^{-1}	Detonation pressure /Pa	Adiabatic index in the initial stage	Adiabatic index in the second stage
3.1×10^6	5×10^3	7×10^9	3.0	1.33

Table 5
Relevant parameters of the rock and the virtual interface used in the numerical simulation.

Density /kg·m^3	Elasticity modulus /Pa	Poisson's ratio	Cohesion /Pa	Tensile strength /Pa
2500	5×10^9	0.25	3×10^6	1×10^7
Internal friction angle /°	Tensile fracture energy /Pa·m	Shear fracture energy /Pa·m	Normal connection stiffness per unit area /GPa·m^{-1}	Tangential connection stiffness per unit area /GPa·m^{-1}
40.0	100	1000	100	100

simulation is carried out by setting the action time of the explosive. When the explosive element elapses for a period of time greater than the blasting action time; the explosive element fails and the gas pressure in the explosive element is zero after the failure, whereupon the blasting pressure calculation is no longer performed. This type of calculation method can better simulate the effect of blasting gas and present the crack propagation process more realistically. However, owing to the sudden unloading of the blasting pressure, the dynamic behavior of the crack in the arrest stage may be inaccurate. The relevant numerical simulation parameters of the explosive in this work are given in Table 4.

The rock model employs an elastic-damage-fracture constitutive model in which a linear elastic constitutive is applied to each finite element and a damage-fracture constitutive is applied to the virtual interface. The strain rate dependece of tensile strength is considered by setting the strain rate enhancement factor of the tensile strength of the target material. The linear elastic constitutive of the element expressed by the incremental method is given as

$$\begin{cases} \Delta\sigma_{ij} = 2G\Delta\varepsilon_{ij} + \left(K - \frac{2}{3}G\right)\Delta\theta\delta_{ij} \\ \sigma_{ij}(t_1) = \Delta\sigma_{ij} + \sigma_{ij}(t_0) \end{cases}, \tag{3}$$

where σ_{ij} is the stress tensor; $\Delta\sigma_{ij}$ and $\Delta\varepsilon_{ij}$ are the incremental stress and strain tensors, respectively; $\Delta\theta$ is the volume strain increment; K and G are the bulk and shear moduli, respectively; δ_{ij} is the Kronecker mark; t_0 is the current time step; and t_1 is the subsequent time step.

The damage and fracture calculation on the virtual interface was carried out using the tensile shear composite constitutive considering the fracture energy. The incremental method was used to calculate the normal and tangential contact stress on the virtual interface at the next time step, which is given as

$$\begin{cases} F_n(t_1) = F_n(t_0) - k_n A_c \Delta du_n \\ F_s(t_1) = F_n(t_0) - k_s A_c \Delta du_s \end{cases}, \tag{4}$$

where F_n and F_s are the normal and tangential connection force on the penalty spring, respectively; k_n and k_s are the normal and tangential connection stiffness per unit area, respectively; A_c is the virtual interface area; and Δdu_n and Δdu_s are the normal and tangential relative displacement increments, respectively.

The relevant parameters of the rock and the virtual interface used in this numerical simulation are given in Table 5.

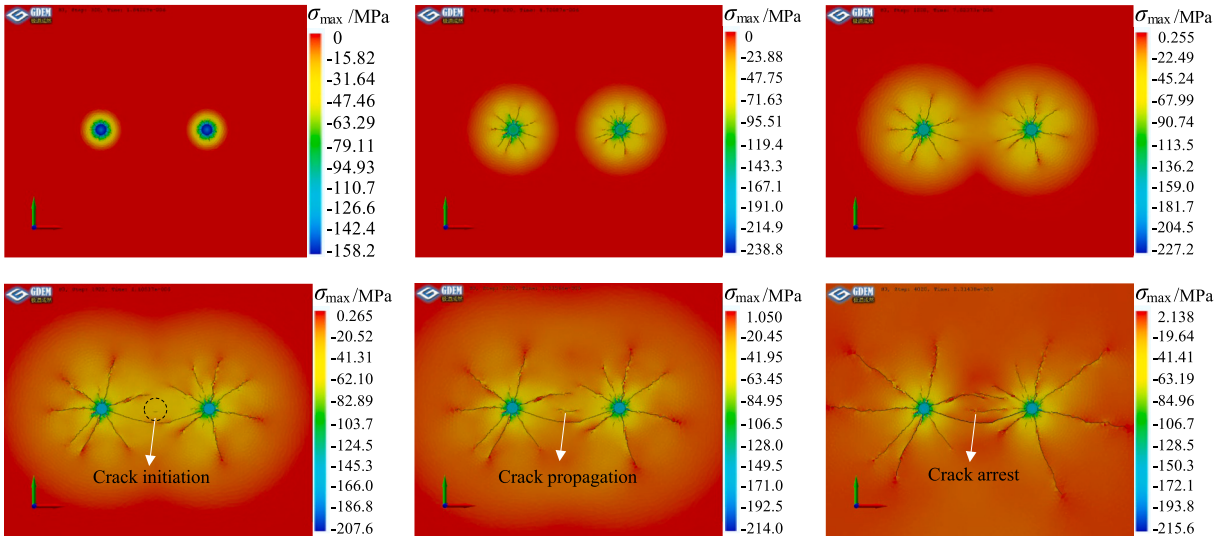

Fig. 10. Evolution of the maximum principal stress and blast-induced crack propagation process for borehole spacing $\Delta l = 60$ mm and simultaneous borehole detonation ($\Delta t = 0$), showing maximum principle stress images (left to right) at $t = 1.84$, 4.72, 7.02 (upper images), 11.05, 13.36, and 23.14 μs (lower images).

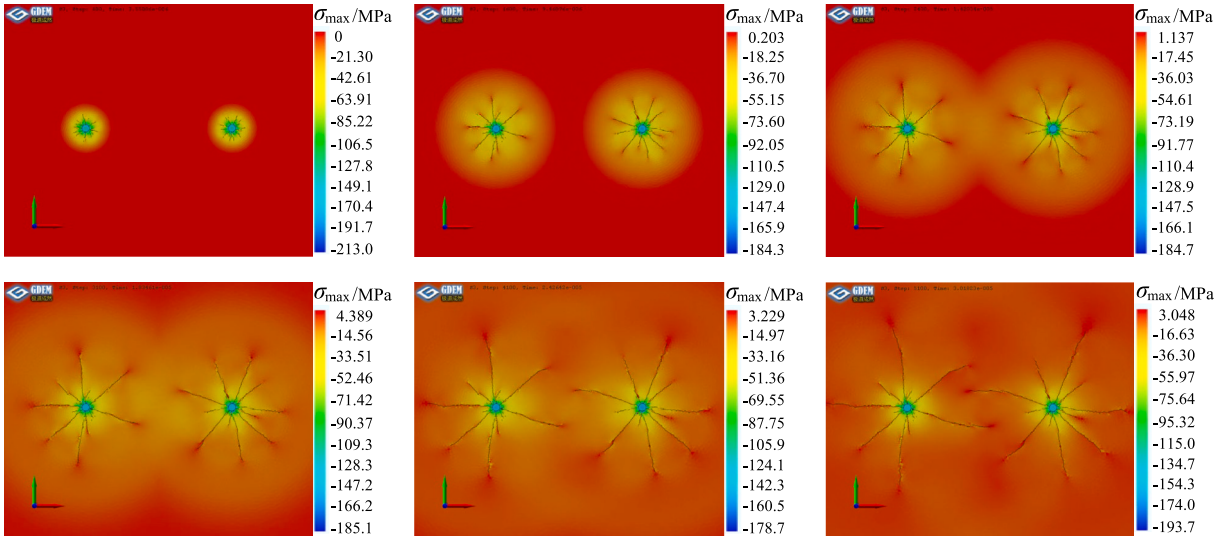

Fig. 11. Evolution of the maximum principal stress and blast-induced crack propagation process for borehole spacing $\Delta l = 120$ mm and simultaneous borehole detonation ($\Delta t = 0$), showing maximum principle stress image (left to right) at $t = 3.55$, 9.46, 14.20 (upper images), 18.35, 24.26, and 30.18 μs (lower images).

4.2. Procedure description

Fig. 10 shows the maximum principal stress evolution and blast-induced crack propagation process with a borehole spacing of $\Delta l = 60$ mm for simultaneous borehole detonation ($\Delta t = 0$). Under the blasting load, when $t = 1.84$ μs, several blast-induced cracks begin to appear around the two boreholes and gradually propagate outward. When $t = 7.02$ μs, the blasting stress waves from the two boreholes begin to meet at the middle position between the two boreholes, and the blast-induced cracks continue to propagate. With the continuous superposition of the blasting stress wave, when $t = 11.05$ μs, crack initiation occurs at the middle position between the two boreholes and the formed crack gradually propagates toward the two boreholes. With subsequent weakening of the stress superposition and dissipation of the blasting energy, the crack at the middle position stops propagating at $t = 23.14$ μs.

Fig. 11 shows the maximum principal stress evolution and blast-induced crack propagation process with a borehole spacing of $\Delta l = 120$ mm. Similar to the results for a borehole spacing of $\Delta l = 120$ mm, after simultaneous detonation of the two boreholes ($\Delta t = 0$) the blasting stress waves generated by the two boreholes propagate outward and the blast-induced cracks generated at the boreholes begin to propagate. When $t = 23.14$ μs, the blasting stress waves from the two boreholes meet and superpose at the middle position between the two boreholes. Thereafter, the blast-induced cracks generated at the two boreholes continue to propagate toward the periphery, and no cracks are generated at the stress wave superposition area between the two boreholes.

4.3. Stress analysis

The stress change at particular gauging points as found by the numerical simulation calculation process was analyzed. Similar to the experimental analysis in Section 3, the midpoint of the two boreholes was labeled as gauging point M'; gauging points on the left side of M′ were labeled L1', L2', …, L6'; and gauging points on the right side of M′ were labeled R1', R2', …, R6'. Additionally, the distance between two adjacent gauging points was 50 mm, and the direction along (perpendicular to) the borehole connection line was designated the *x*- (*y*-)

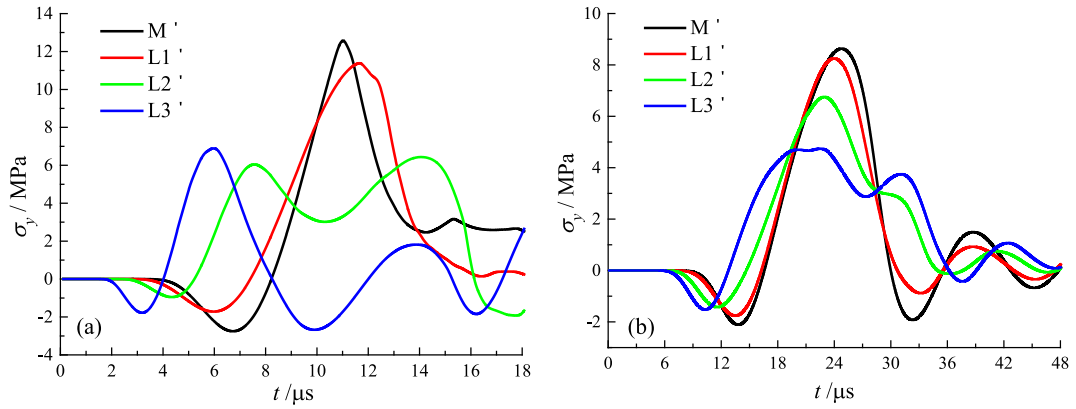

Fig. 12. Numerical simulation of the stress component σ_y vs. time after simultaneous borehole detonation ($\Delta t = 0$) for borehole spacing Δl= (a) 60 and (b) 120 mm.

direction. The analysis results of the model experiments detailed in Section 4.1 show that, in the stress wave superposition area between the two boreholes, the stress component in the *x*-direction was mainly compressive stress, while that in the *y*-direction was mainly tensile stress. In rock blasting, crack propagation in areas far from the borehole is dominated by tensile stress. Therefore, the evolution characteristics of the stress component σ_y in the *y*-direction were mainly analyzed herein, and Fig. 12 shows the stress component σ_y as a function of time after detonation for the two numerical simulations of $\Delta l = 60$ and 120 mm.

When the borehole spacing is $\Delta l = 60$ mm, the blasting stress waves from the two boreholes superposed at the middle of the connection line of the two boreholes (i.e., $x = 0$, $y = 0$) and the tensile stress was significantly enhanced. The peak value of σ_y at gauging points M' (i.e., $x = 0$) and L1' (i.e., $x = -50$ mm) are 12.32 and 11.39 MPa, respectively, which are greater than the tensile strength of the rock (10 MPa). Therefore, the rock undergoes tensile fracture, and a crack initiates at the middle of the connection line of the two boreholes, as shown in Fig. 10. However, the range and extent of stress wave superposition are limited. The peaks of σ_y of gauging points L2' (i.e., $x = -100$ mm) and L3' (i.e., $x = -150$ mm) are 6.55 and 6.90 MPa, respectively, which are less than the tensile strength of rock and do not satisfy the basic conditions of crack initiation and propagation. The crack is generated at the middle of the connection line of the two boreholes and propagates to the two boreholes, but the propagation length is limited to a final length of 18 mm (Fig. 10).

When the borehole spacing is $\Delta l = 120$ mm, the peak value of σ_y of gauging points M′, L1', L2' and L3' are 8.63, 8.25, 6.75 and 4.70 MPa, respectively. Owing to the relatively large borehole spacing, the peak σ_y values at these gauging points are significantly smaller than those at the corresponding gauging points for a borehole spacing of $\Delta l = 60$ mm. Among the gauging points, the peak σ_y value of the gauging point M′ is the largest. Further, although stress wave superposition increases the peak of σ_y, its value remains smaller than the tensile strength of the rock and crack initiation does not occur in the middle of the connection line of the two boreholes.

We found that crack initiation can occur in the stress wave superposition area between two boreholes, but there exist relatively stringent requirements for the explosive parameters, rock properties and borehole spacing. In the case in which the explosive parameters and rock properties are determined, a large borehole spacing will rapidly attenuate the blasting stress in the specimen. Thus, the superposed tensile stress will be less than the tensile strength of the specimen, and it will be difficult to form new cracks in the stress wave superposition area. When the borehole spacing is small, although the tensile stress in the stress wave superposition area may exceed the tensile strength of the specimen, the initial blast-induced cracks generated at the borehole will rapidly propagate to the stress wave superposition area. This causes new cracks in the stress wave superposition area to generate too late (i.e., be "submerged") in the blast-induced cracks that propagate from the two boreholes.

5. Conclusions

In the stress wave superposition area between two detonation boreholes, the stress component in the direction of the connection line of the two boreholes is mainly compressive, while that in the direction perpendicular to connection line of the two boreholes is mainly tensile.

When two boreholes are simultaneously detonated, the stress component peak exhibits a "W"-type distribution at gauging points along the connection line of the two boreholes. The stress wave superposition has a stronger effect on the stress component in the direction of the connection line of the two boreholes (mainly compressive stress) than that in the direction perpendicular to the connection line of the two boreholes (mainly tensile stress). These experimental results show that the superposition of blasting stress waves between the two boreholes does not significantly enhance the tensile stress. Although the superposition of blasting stress waves between the boreholes is significantly enhanced for the compressive stress, it is still much smaller than the compressive strength of the specimen, and it is difficult to change the failure mode of the specimen from tensile failure to compression failure. When the detonation of the two boreholes is delayed, the superposition of blasting stress waves between the boreholes exhibits a similar trend to that of simultaneous blasting. With increasing detonation delay time, the position where the two blasting stress wave columns meet gradually moves toward the secondarily-detonated borehole. Further, the stress peak of the stress wave superposition area initially decreases and then increases, and the stress wave of the secondarily-detonated borehole gradually strengthens the stress superposition between the boreholes.

Numerical simulations based on CDEM reproduce the crack initiation process in the stress wave superposition area between the two boreholes. The analysis shows that, in the case where the explosive parameters and rock properties are determined, a borehole spacing that is too large or too small reduces the likelihood of crack initiation in the stress wave superposition area. Crack initiation and propagation in the stress wave superposition area between the two boreholes have relatively stringent requirements for the explosive parameters, rock properties and borehole spacing, which makes it difficult to observe this phenomenon in engineering practice and model experiments.

Compliance with ethics guidelines

Chenxi Ding, Renshu Yang and Chun Feng declare that they have no conflict of interest or financial conflicts to disclose.

Declaration of competing interest

The authors declare that they have no known competing financial interests or personal relationships that could have appeared to influence the work reported in this paper.

Acknowledgments

This research was supported by: (1) the National Natural Science Foundation of China (51934001); (2) 2020 annual Open Fund of Failure Mechanics & Engineering Disaster Prevention and Mitigation, Key Laboratory of Sichuan Province, Sichuan University, (2020JDS0022); (3) China Postdoctoral Science Foundation (2020M680354).

References

1 Li M, Zhu ZM, Liu RF, Liu B, Zhou L, Dong YQ. Study of the effect of empty holes on propagating cracks under blasting loads. *Int J Rock Mech Min Sci*. 2018;103:186–194.
2 Silva JD, Amaya JG, Basso F. Development of a predictive model of fragmentation using drilling and blasting data in open pit mining. *J South Afr I Min Metall*. 2017;117(11):1089–1094.
3 Mohammad BK, Robert H. Processing of measurement while drilling data for rock mass characterization. *Int J Rock Mech Min Sci*. 2016;26(6):989–994.
4 Xie LX, Lu WB, Zhang QB, Jiang QH, Wang GH, Zhao J. Damage evolution mechanisms of rock in deep tunnels induced by cut blasting. *Tunn Undergr Space Technol*. 2016;58:257–270.
5 Ocak I, Bilgin N. Comparative studies on the performance of a roadheader, impact hammer and drilling and blasting method in the excavation of metro station tunnels in Istanbul. *Tunn Undergr Space Technol*. 2010;25(2):181–187.
6 Lu WB, Chen M, Geng X, Shu DQ, Zhou CB. A study of excavation sequence and contour blasting method for underground powerhouses of hydropower stations. *Tunn Undergr Space Technol*. 2012;29(29):31–39.
7 Li HB, Xiang X, Li JC, Zhao J, Liu B, Liu YQ. Rock damage control in bedrock blasting excavation for a nuclear power plant. *Int J Rock Mech Min Sci*. 2011;48(2):210–218.
8 Katsabanis PD. Analysis of the effects of blasting on comminution using experimental results and numerical modelling. *Rock Mech Rock Eng*. 2020;53:3093–3109.
9 Cho SH, Min HD, Park JH, et al. Full scaled-column blast experiments for investigating the influence of the stemming materials on the column fragmentation in explosive demolition. *Sci Technol Energetic Mater*. 2010;71(5-6):123–128.
10 Zhu ZM, Xie HP, Mohanty B. Numerical investigation of blasting-induced damage in cylindrical rocks. *Int J Rock Mech Min Sci*. 2008;45:111–121.
11 Rossmanith HP. The use of Lagrange diagrams in precise initiation blasting. Part I: two interacting blastholes. *Fragblast*. 2002;6(1):104–136.
12 Rossmanith HP, Kouzniak N. Supersonic detonation in rock mass - Part 2: particle displacements and velocity fields for single and multiple non-delayed and delayed detonating blastholes. *Fragblast*. 2004;8(2):95–117.
13 Vanbrabant F, Espinosa A. Impact of short delays sequence on fragmentation by means of electronic detonators: theoretical concepts and field validation. In: *Fragblast 8. Proceedings of the 8th International Symposium on Rock Fragmentation by Blasting*. Santiago: Editec SA; 2006:326–331.
14 Cho SH, Nakamura Y, Mohanty B, Yang HS, Kaneko K. Numerical study of fracture plane control in laboratory-scale blasting. *Eng Fract Mech*. 2008;75:3966–3984.
15 McKinstry R, Floyd J, Bartley D. Electronic detonator performance evaluation. In: *Proceedings of the 28th Annual Conference on Explosives and Blasting Technique*. Las Vegas; 2002:1–20.
16 Lewis N, Pereira P. Operating improvements at Vuloan Materials McCook quarry using electronic detonators. In: *Proceedings of the 29th Annual Conference on Explosives and Blasting Technique*. Nashville; 2003:1–14.
17 Khandelwal M, Singh TN. Prediction of blast-induced ground vibration using artificial network. *Int J Rock Mech Min Sci*. 2009;46(7):1214–1222.
18 Katsabanis PD, Tawadrous A, Braun C, Kennedy C. Timing effects on the fragmentation of small scale blocks of granodiorite. *Fragblast*. 2006;10(1-2):83–93.
19 Katsabanis PD, Omidi O. The effect of the delay time on fragmentation distribution through small-and medium-scale testing and analysis. In: *Proceedings of 11th International Symposium on Rock Fragmentation by Blasting (Fragblast 11), Sydney, Australia*. 2015:24–26.
20 Blair DP. Limitations of electronic delays for the control of blast vibration and fragmentation. In: *Pro-ceedings of the 9th International Symposium on Rock Fragmentation by Blasting. Sept, Granada, Spain*. 2010.
21 Johansson D. Shock wave interactions in rock blasting: the use of short delays to improve fragmentation in model-scale. *Rock Mech Rock Eng*. 2013;46(1):1–18.
22 Yi CP, Johansson D, Nyberg U, Beyglou A. Stress wave interaction between two adjacent blast holes. *Rock Mech Rock Eng*. 2016;49(5):1803–1812.
23 Sjöberg J, Schill M, Hilding D, Yi CP, Nyberg U, Johansson D. Computer simulations of blasting with precise initiation. In: *Rock Engineering and Technology for Sustainable Underground Construction. Proceedings, Eurock 2012-ISRM International Symposium, Stockholm*. May 2012:28–30.
24 Yue ZW, Yang LY, Wang YB. Experimental study of crack propagation in polymethyl methacrylate material with double holes under the directional controlled blasting. *Fatig Fract Eng Mater Struct*. 2013;36(8):827–833.
25 Wang YB, Yang RS, Ding CX, Chen C, Zuo JJ. Dynamic caustics experiment on crack propagation of defective medium under the effect of explosive stress waves of double holes. *J China Coal Soc*. 2016;41(7):1755–1761 ([in Chinese]).
26 Peters WH, Ranson WF. Digital imaging techniques in experimental stress analysis. *Opt Eng*. 1982;21(3):427–431.
27 Chu TC, Ranson WF, Sutton MA. Applications of digital-image-correlation techniques to experimental mechanics. *Exp Mech*. 1985;25(3):232–244.
28 Tiwari V, Sutton MA, McNeill SR, et al. Application of 3D image correlation for full-field transient plate deformation measurements during blast loading. *Int J Impact Eng*. 2009;36:862–874.
29 Yang RS, Ding CX, Yang LY, Lei Z, Zheng CD. Study of decoupled charge blasting based on high-speed digital image correlation method. *Tunn Undergr Space Technol*. 2019;83:51–59.
30 Li SH, Wang JG, Liu BS, Dong DP. Analysis of critical excavation depth for a jointed rock slope using a face-to-face discrete element method. *Rock Mech Rock Eng*. 2007;40(4):331–348.
31 Wang YN, Zhao MH, Li SH, Wang JG. Stochastic structural model of rock and soil aggregates by continuum-based discrete element method. *Sci China E*. 2005;48(S1):95–106.
32 Feng C, Li SH, Hao WH, Ge W. Numerical simulation for penetrating and blasting process of EPW based on CDEM. *J Vib Shock*. 2017;36(13):11–18 ([in Chinese]).